Identification of volcanic rootless cones, ice mounds, and impact craters on Earth and Mars: Using spatial distribution as a remote sensing tool

B. C. Bruno,[1] S. A. Fagents,[1] C. W. Hamilton,[1] D. M. Burr,[2] and S. M. Baloga[3]

Received 16 June 2005; revised 29 March 2006; accepted 10 April 2006; published 27 June 2006.

[1] This study aims to quantify the spatial distribution of terrestrial volcanic rootless cones and ice mounds for the purpose of identifying analogous Martian features. Using a nearest neighbor (NN) methodology, we use the statistics R (ratio of the mean NN distance to that expected from a random distribution) and c (a measure of departure from randomness). We interpret R as a measure of clustering and as a diagnostic for discriminating feature types. All terrestrial groups of rootless cones and ice mounds are clustered (R: 0.51–0.94) relative to a random distribution. Applying this same methodology to Martian feature fields of unknown origin similarly yields R of 0.57–0.93, indicating that their spatial distributions are consistent with both ice mound or rootless cone origins, but not impact craters. Each Martian impact crater group has $R \geq 1.00$ (i.e., the craters are spaced at least as far apart as expected at random). Similar degrees of clustering preclude discrimination between rootless cones and ice mounds based solely on R values. However, the distribution of pairwise NN distances in each feature field shows marked differences between these two feature types in skewness and kurtosis. Terrestrial ice mounds (skewness: 1.17–1.99, kurtosis: 0.80–4.91) tend to have more skewed and leptokurtic distributions than those of rootless cones (skewness: 0.54–1.35, kurtosis: −0.53–1.13). Thus NN analysis can be a powerful tool for distinguishing geological features such as rootless cones, ice mounds, and impact craters, particularly when degradation or modification precludes identification based on morphology alone.

Citation: Bruno, B. C., S. A. Fagents, C. W. Hamilton, D. M. Burr, and S. M. Baloga (2006), Identification of volcanic rootless cones, ice mounds, and impact craters on Earth and Mars: Using spatial distribution as a remote sensing tool, *J. Geophys. Res.*, *111*, E06017, doi:10.1029/2005JE002510.

1. Introduction

[2] The objective of this research is to refine and apply the nearest neighbor (NN) technique used by *Bruno et al.* [2004] to distinguish among different origins for small (less than a few km), circular to elongate, positive-relief mounds and cones, for the purposes of understanding the local geology and, ultimately, constructing a historical volatile inventory for our study sites on Mars. Geologic features that form in the presence of water or ice are of key interest because they provide information about the abundance and spatial distribution of volatiles on Mars at the time of feature formation. Such features include volcanic rootless cones, subglacial volcanoes, rampart craters, pingos, and other types of ice mounds [*Carr et al.*, 1977; *Allen*, 1979a, 1979b; *Frey et al.*, 1979; *Lucchitta*, 1981; *Frey and Jarosewich*, 1982; *Mouginis-Mark*, 1987; *Cabrol et al.*, 2000; *Chapman and Tanaka*, 2001]. Water-rich localities on Mars not only represent potential niches for past biological development, but they are also prospective sources of water for future Mars missions.

[3] Rootless volcanic cones are an important diagnostic of ice distribution in the near-surface regolith [*Greeley and Fagents*, 2001; *Lanagan et al.*, 2001; *Fagents et al.*, 2002; *Fagents and Thordarson*, 2006]. They were first identified in Viking Orbiter imagery [*Allen*, 1979a; *Frey et al.*, 1979; *Frey and Jarosewich*, 1982], and more recently from data acquired by both the Thermal Emission Imaging System (THEMIS) on Mars Odyssey and the high-resolution (Narrow-Angle) Mars Orbiter Camera (MOC-NA) aboard Mars Global Surveyor. Rootless cones, found in abundance in Iceland, form when lava flowing in an inflating pahoehoe flow field interacts explosively with water or ice contained within the substrate [*Thorarinsson*, 1951, 1953]. Successive explosive pulses eject fragments of lava and substrate from the explosion site to build a cratered cone of ash, scoria, spatter, and clastic substrate sediments. Once activity at a given explosion site wanes (due to volatile depletion or a cessation of lava supply), explosive interactions typically initiate nearby. The result is a group containing tens to

[1] Hawai`i Institute of Geophysics and Planetology, University of Hawai`i, Honolulu, Hawaii, USA.
[2] SETI Institute, Mountain View, California, USA.
[3] Proxemy Research, Bowie, Maryland, USA.

0148-0227/06/2005JE002510

hundreds of cones [*Thordarson et al.*, 1998; *Thordarson*, 2000].

[4] Rootless volcanic cones are distinct from primary scoria cones, which form over a volcanic conduit more deeply rooted in the crust to a magma source. Unlike primary cones, rootless cones are not the source of lava flows (although they can feed rheomorphic flows that can be difficult to distinguish from primary lava flows). Figures 1a and 1b show a typical rootless cone group within the 1783-84 Laki lava flow in Iceland. The morphology and spatial density of rootless cones provide an indication of the quantity and location of water in the substrate at the time of cone formation; modeling the dynamics of cone-forming explosions permits assessment of the vapor mass and pressure required to produce cones of the observed numbers and sizes [*Greeley and Fagents*, 2001]. If rootless cones can be unequivocally identified on Mars, we will have a powerful means to gauge the amount, distribution, and evolution of near-surface volatiles in the regolith.

[5] Similarly, the putative identification of pingos and other ice mounds on Mars implies the presence of volatiles in the Martian regolith [*Lucchitta*, 1981; *Parker et al.*, 1993; *Cabrol et al.*, 2000; *Burr et al.*, 2005; *Soare et al.*, 2005]. A pingo is a type of ice cored mound, common in periglacial environments within Alaska, Canada, and Russia. Like rootless cones, pingos can grow up to several hundreds of meters in basal diameter and up to tens of meters in height [*Washburn*, 1973].

[6] In general, pingos form when the overburden is domed above a segregated ice body that grows either by (1) intrusion and subsequent freezing of liquid water injected into permafrost; (2) progressive underplating of an ice cored mound as an underlying water reservoir freezes; or (3) a combination of both these processes [*Washburn*, 1973; *Mackay*, 1987]. Depending on their formation mechanism, pingos are divided into two main categories: hydrostatic and hydraulic.

[7] The majority of terrestrial pingos are hydrostatic (“closed-system”) pingos and form in response to the draining of ephemeral ponds and lakes which exposes the unfrozen basin to subfreezing temperatures [*Porsild*, 1938; *Müller*, 1959; *Mackay*, 1962, 1973, 1979, 1998; *Washburn*, 1973]. Progradation of the freezing front both from the ground surface downward and the underlying permafrost upward pressurizes the residual pore water. In transmissive sediments, this pore water flows ahead of the freezing front toward the basin center, the usual site of minimal permafrost growth. Continued flow and freezing of this expelled pore water, in addition to a small effect from volumetric expansion, domes up the overlying permafrost layer to form a mound [*Mackay*, 1998; *Burr et al.*, 2005]. Continued growth can produce radial tension fractures from the summit and circumferential compression fractures at the margins. Pingo collapse may occur when the summit ruptures and the remaining liquid water below the ice mound escapes. Collapsed pingos typically form a depression surrounded by a raised ring of residual sediment. Figures 1c and 1d show hydrostatic pingos from the Tuktoyaktuk Peninsula, Canada.

[8] Hydraulic (“open-system”) pingos tend to form in narrow valleys or on slopes in areas of discontinuous (or locally thinner) permafrost. In these cases, artesian pressure forces water to intrude into shallow permafrost. Upon freezing, the water ice uplifts the overburden to form mounds [*Washburn*, 1973]. Hydraulic pingos may also grow as a result of hydraulic lift, where low artesian pressure is amplified through confinement under a pingo [*Müller*, 1959; *Holmes et al.*, 1968]. When discussing ice cored mounds of uncertain origin, we use the general term “ice mound” (rather than the specific term “pingo”) to include other segregated ice bodies such as palsas, hydrolaccoliths, icings, and ice hummocks. (See *Washburn* [1973] for a comprehensive description of these features.) We reserve the term “pingo” for ice cored mounds of known hydraulic or hydrostatic origin.

[9] On Mars, potential rootless volcanic cones have been identified in the northern lowland plains (Figure 2a), including Acidalia, Amazonis, Isidis, and Elysium Planitiae [*Allen*, 1979a; *Frey and Jarosewich*, 1982; *Greeley and Fagents*, 2001; *Lanagan et al.*, 2001; *Fagents et al.*, 2002]. Possible Martian ice mounds have been identified in Gusev Crater, Athabasca Valles and the Cerberus Plains (Figure 2b) as defined by *Plescia* [1990], and Chryse, Acidalia, and Utopia Planitiae [*Lucchitta*, 1981; *Parker et al.*, 1993; *Cabrol et al.*, 2000; *Burr et al.*, 2005; *Soare et al.*, 2005; *Page and Murray*, 2006].

[10] Historically, Martian pingos have been difficult to identify on the basis of Viking Orbiter data, in part because of limited availability of high-resolution images, but also because only the most mature pingos exhibit distinctive morphologies. Younger and/or smaller pingos are typically expressed as low-relief mounds. Only once the mound is sufficiently upheaved does its surface begin to rupture, thereby exposing the interior ice, which melts or sublimes to form crevices and pits at or near the summit [*Washburn*, 1973; *Mackay*, 1979]. Moreover, these morphologies are apt to be confused with those of rootless cones, and the presence of pingos or other ice mounds on Mars remains equivocal [*Theilig and Greeley*, 1979; *Lucchitta*, 1981; *Rossbacher and Judson*, 1981; *Squyres et al.*, 1992; *Parker et al.*, 1993; *Cabrol et al.*, 2000].

[11] Geological context is therefore of key importance in identifying rootless cones and ice mounds. Interpretation of a volcanic origin is relatively straightforward for pristine cones lying on surfaces with clear textural indications of lava flow morphology [*Lanagan et al.*, 2001]. However, in areas where the cones and/or the underlying surface are degraded or mantled by dust, or for which image resolution is a limiting factor, it becomes harder to identify the origins on the basis of morphology alone. Ambiguities arise because, under these adverse conditions, other small, circular, pitted cones or mounds can resemble rootless cones. In addition to the ice mound hypothesis, other possibilities include (1) secondary (Figure 2c) or pedestal (Figure 2d) impact craters, the latter having resistant ejecta armoring a more easily eroded substrate; (2) mud volcanoes produced by gas- or water-charged eruptions of clastic sediments [*Tanaka*, 1997; *Farrand et al.*, 2005]; (3) primary scoria cones; (4) gravity craters, produced when blocks of ice transported by jökulhlaups (glacial outburst floods) settle into soft sediments [*Gaidos and Marion*, 2003]; and (5) kettle holes, which are formed when sediment-laden ice blocks are partially buried and subsequently melted [*Gaidos and Marion*, 2003].

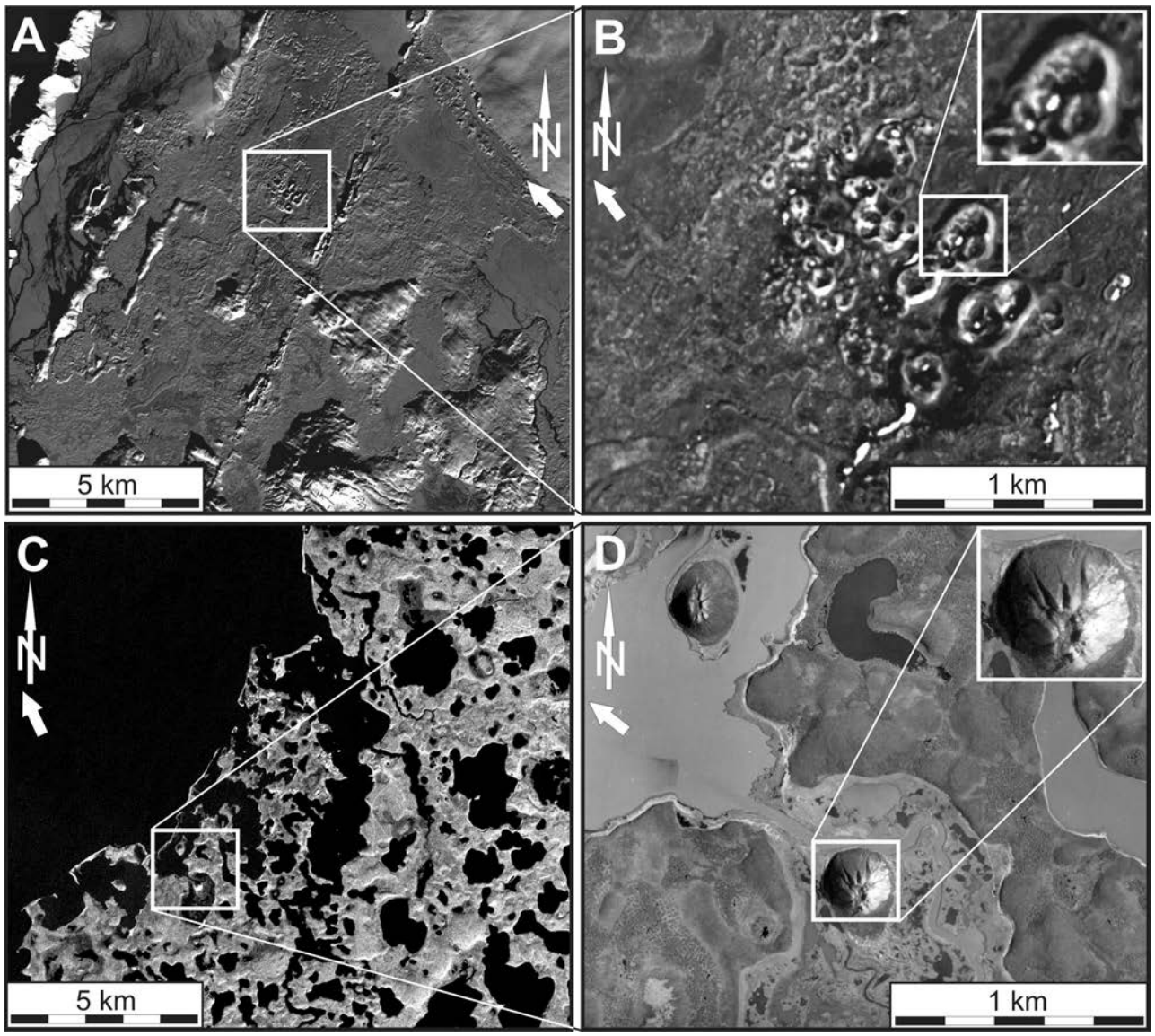

Figure 1. Terrestrial rootless cone groups (RCGs) and pingos. (a) RCGs are common in the 1783-84 Laki lava flow, Iceland (Advanced Spaceborne Thermal Emission and Reflection Radiometer (ASTER) image AST_L1B_003_11072002125225_11212002071251, Band 1 (0.5560 μm), 15 m/pixel). (b) Magnified view of Innri Eyrar, a RCG located to the west of the Laki fissure (Air photo 2408, Icelandic Geodetic Survey, Akranes). (c) The Tuktoyaktuk Peninsula, Northwest Territories, Canada, includes the largest concentration of pingos on Earth (Landsat 7 ETM+ image LE7063011000224950, Panchromatic (0.5–0.9 μm), 15 m/pixel). (d) Magnified view depicting two prominent pingos: Ibyuk Pingo (inset) and Split Pingo (Air photo A27917-35-1993, National Air Photo Library, Ottawa). The illumination direction (180° from sun azimuth angle) is indicated by the broad white arrow.

[12] Even where the morphology is well expressed, interpretations are not unequivocal because there are no definitive morphological criteria for many of these feature types. For example, there are various degrees of overlap between the different feature types in parameters such as basal diameter, height, crater (or pit) diameter, and ratio of crater (or pit) diameter to cone diameter [*Frey et al.*, 1979; *Frey and Jarosewich*, 1982; *Greeley and Fagents*, 2001]. Moreover, even if a set of identifying morphological criteria were developed, it is commonly not possible to acquire the necessary measurements for the Martian cases due to data limitations (e.g., availability of high spatial resolution images, inadequate topographic information). Finally, the low-gravity, low-atmospheric pressure environment on Mars can exert strong controls on eruptive behavior and cone (or ice mound) growth. Morphologies quite different from terrestrial analogs could be produced for the same formation conditions. For example, in the case of rootless explosions, the Martian low gravity and low atmospheric pressure act to produce more highly explosive interactions, more widely distributed eruptive products, and hence broader, shallower cones [*Greeley and Fagents*, 2001; *Fagents et al.*, 2002; *Fagents and Thordarson*, 2006].

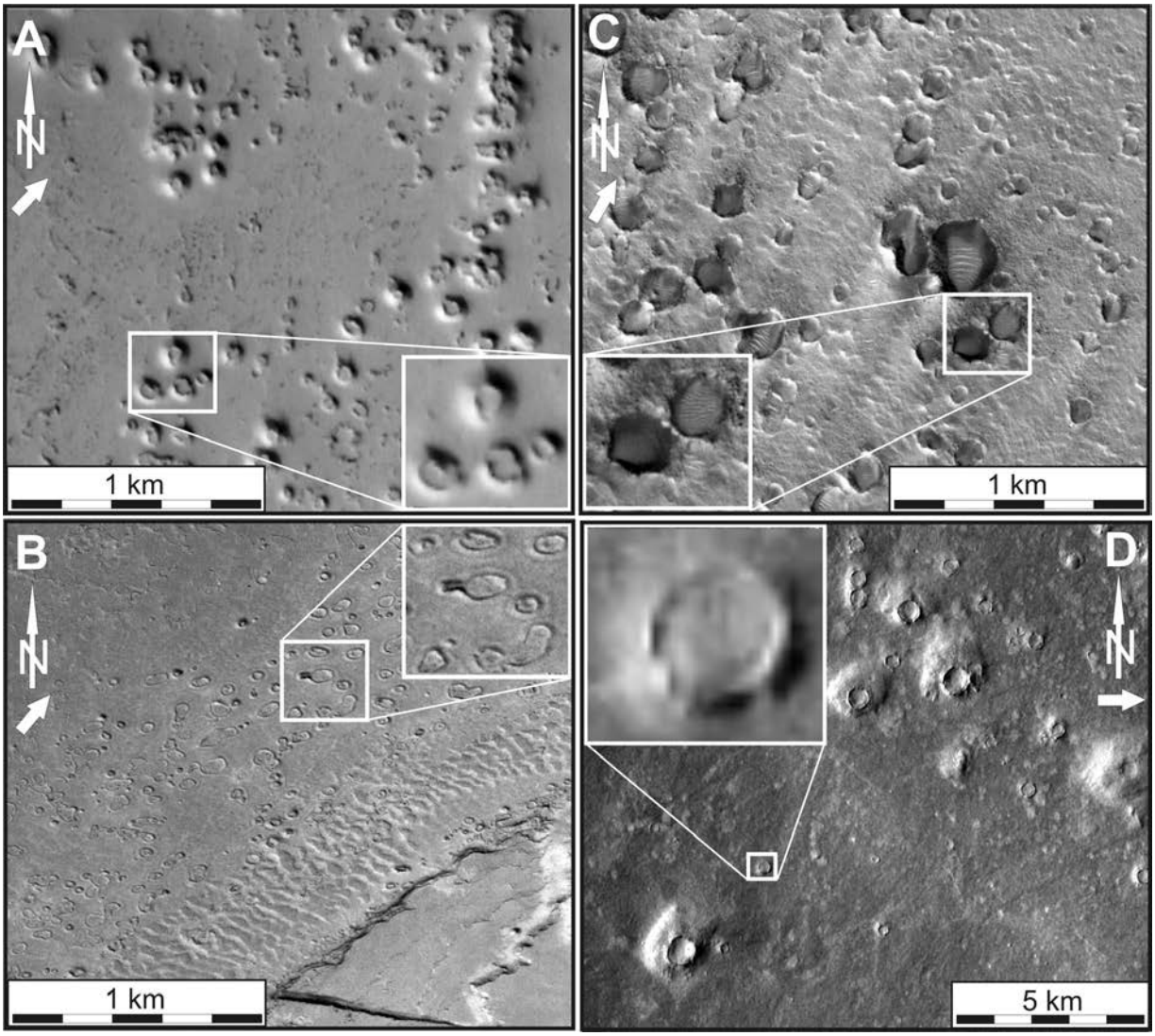

Figure 2. Feature fields on Mars. (a) Candidate rootless cone group (RCG) southeast of Phlegra Montes (MOC-NA image M08-01962, 4.52 m/pixel). (b) Candidate Martian group (may represent rootless cones or ice mounds) in western Cerberus Planitia (MOC-NA image E10-01384, 3.09 m/pixel). (c) Secondary impact craters northeast of Mars Pathfinder site in Ares Vallis (MOC-NA image R10-05447, 3.13 m/pixel). (d) Pedestal craters east of Acidalia Planitia (THEMIS visible image V1358002, 19 m/pixel). The illumination direction (180° from sun azimuth angle) is indicated by the broad white arrow. Note: Figures 1a, 1c, and 2d; Figures 1b, 1d, and 2a–2c; and insets for Figures 1b, 1d, and 2a–2d are represented to the same scale, respectively.

[13] Given these interpretive difficulties, *Bruno et al.* [2004] developed and applied a suite of nonmorphological statistical criteria to quantify the distribution of small, circular structures within a feature field on the basis of NN analysis and linear alignment detection techniques. They applied these techniques to rootless cone groups in Iceland, candidate rootless cone groups on Mars, and impact craters on Mars of probable secondary origin. They found that the spatial relationships of Martian candidate rootless cones are indistinguishable from those of Icelandic rootless cones (i.e., they both show similar degrees of clustering within their groups), but are markedly different from those of Martian impact craters (which show no evidence of intrafield clustering). This suggests that we can have some confidence in distinguishing rootless cones from impact craters in images where morphology is not well defined due to degradation, modification or sediment cover. Other investigators have similarly investigated clustering of primary volcanic cones, on the basis of qualitative observations, cluster analysis and related NN-based techniques [*Carr*, 1976; *Settle*, 1979; *Heming*, 1980; *Walker*, 1981; *Hasenaka and Carmichael*, 1985a, 1985b; *Connor*, 1990; *Connor et al.*, 1992; *Connor and Hill*, 1995], but we are not aware of any other comparable published studies that relate to the feature types included in this study.

[14] We recognize some limitations of the NN technique as applied by *Bruno et al.* [2004]. First, the NN technique requires that an envelope be drawn to enclose the feature

Table 1. Terrestrial Rootless Cone Groups, Iceland[a]

	Air Photo Number and Position of Feature Field	Air Photo Scale	Location
	Laki Lava Flow (1783–84)		
Blagil	1869 – Just NE of center	1:37000	64.0°N, 18.4°W
Innri Eyrar (Figure 1)	2408 – Just E of center	1:37000	64.2°N, 18.2°W
Hnuta (North)	1870 – Eastern 1/3 of image	1:37000	64.0°N, 18.4°W
Hnuta (South)	1870 – Eastern 1/3 of image	1:37000	64.0°N, 18.4°W
Trollhamar	2408 – Northern edge of image	1:37000	64.2°N, 18.2°W
Stakafell	2409 – Just SW of center	1:37000	64.2°N, 18.2°W
	Eldgja Lava Flow (1.1 kybp)		
Landbrot	1413 – Northern half of image	1:37000	63.7°N, 18.1°W
	Leitin Lava Flow (4.6 kybp)		
Raudholar	264 – Center of image	1:16000	64.1°N, 21.7°W

[a]Air photos obtained from Geodetic Survey of Iceland.

field. *Bruno et al.* [2004] used the best fitting rectangle to enclose all cones or craters in a given group, but there are a number of reasons why this is not the best approach (as discussed below). Second, features which occur along the border of an image were fully included as members of the group. However, our inability to assess their nearest neighbors (which might be beyond the edge of the image) suggests that they should be selectively excluded from the analysis. The third issue is group definition. Several feature fields contain subclusters within them, and treating all features as a single group can considerably affect NN results. Finally, and perhaps most important, standard NN methodology reduces all the information of a feature field to two statistics (R and c), and much important information is lost in this process.

[15] In this paper we present refinements to standard NN methodology in the areas outlined above, and this leads to a more objective assessment of spatial distribution. We apply our methodology to the same data set studied by *Bruno et al.* [2004], as well as to terrestrial ice mounds, candidate Martian ice mounds, and Martian pedestal craters for the first time. Finally, we outline a skewness-kurtosis analysis which, when combined with the standard NN statistics R and c, proves useful in separating feature types.

[16] Throughout this paper, we use the term "random." Spatial randomness is defined for a set of points on a given area as follows: "any point has had the same chance of occurring on any subarea as any other point; that any subarea of specified size has had the same chance of receiving a point as any other subarea of that size, and that the placement of each point has not been influenced by that of any other point" [*Clark and Evans*, 1954]. Thus spatial randomness is intimately connected with a Poisson probability distribution of points in a plane of infinite extent. In this work, we are concerned only with spatial randomness resulting from an underlying Poisson distribution and its corresponding probability distribution of nearest neighbor distances. Therefore we use the term "random" as a convenient shorthand for these concepts.

2. Data

2.1. Icelandic Rootless Cones (8 Groups)

[17] For our first data set, we apply our refined NN methodology to the same three Icelandic lava flow fields (Laki, Eldgjá, and Leitin) previously considered by *Bruno et al.* [2004]. Within these three flow fields are multiple distinct rootless cone groups, of which we analyze eight (Table 1). Two of these (Hnuta North and Hnuta South) were previously considered to be a single group; *Bruno et al.* [2004] listed only seven rootless cone groups. However, our refined NN technique (detailed below) requires that these two groups be considered separately because they are physically separated by a scarp.

[18] These volcanic cone groups have all been unambiguously determined from field investigations to be rootless cones formed by hydrovolcanic explosions and constructed on top of the host lava flow [*Thoroddsen*, 1894; *Thorarinsson*, 1951; 1953]. In all cases, locations of rootless cones were determined from stereo aerial photographs at scales of 1:37000 (Laki, Eldgjá) and 1:16000 (Leitin). Cone morphology and dimensions vary considerably, as does the spatial distribution of cones within a cone group. Cone basal diameters lie in the 5–450 m range, and cone heights are 2–40 m [*Thorarinsson*, 1953; *Thordarson et al.*, 1992; *Thordarson and Höskuldsson*, 2002].

2.2. Ice Mounds in Canada and Alaska (7 Groups)

[19] Our second data set comprises seven groups of ice mounds in Canada and Alaska (Table 2). These mounds have been mapped by previous authors from stereo aerial photographs and through field investigations, and our analysis is based on their published maps in three locations: Tuktoyaktuk Peninsula area, Northwest Territories, Canada [*Mackay*, 1998]; Tanacross, central Alaska [*Holmes et al.*, 1968] and Prudhoe Bay, northern Alaska [*Walker et al.*, 1985]. The sizes of ice mounds are comparable to those of rootless cones. Basal diameter and height ranges are respectively ~5–600 m and ~3–70 m [*Washburn*, 1973].

[20] In the Tuktoyaktuk Peninsula area, the type locality for hydrostatic pingos, nearly 1400 pingos of greatly varying sizes are divided into three geographic groups, whose boundaries are determined by the peninsular coastline. Basal diameters range from 30 to 600 m and heights range from 3 to ~50 m [*Holmes et al.*, 1968]. In contrast, the Tanacross ice mounds (which are treated as one group) are hydraulic pingos. They can be circular, elliptical, or irregularly shaped. With basal diameters of 15–450 m and heights of 3–30 m, the Tanacross pingos do not attain the sizes of the largest Tuktoyaktuk pingos [*Holmes et al.*,

Table 2. Terrestrial Ice Mound Groups, Canada and Alaska

	Map Source and Position of Feature Field	Map Scale	Location
Tuktoyaktuk area, Canada	*Mackay* [1998]	1:1000000	
Western	– W of Mackenzie River East Channel		69.2°N, 134.5°W
Central	– E of Mackenzie River East Channel; W of Husky Lakes		69.5°N, 132.3°W
Eastern	– E of Husky Lakes		69.5°N, 131.0°W
Tanacross, central Alaska	*Holmes et al.* [1968] – entire map	1:870000	63.5°N, 142.2°W
Prudhoe Bay, northern Alaska	*Walker et al.* [1985]	1:670000	
Steep-sided pingos	– Entire map		70.2°N, 148.5°W
Eastern broad-based mounds	– Eastern half of map		70.1°N, 147.7°W
Western broad-based mounds	– Western half of map		70.3°N, 149.4°W

1968]. Yet the average size (10 or 15 m high, 150 or 200 m wide) of the two groups appears to be about the same [*Stager*, 1956]. Most of the Tanacross pingos lie along gentle to moderate south-facing slopes or on very gently sloping valley floors. None are observed in drained or shallow lake basins, despite an abundance of such basins on the valley floor [*Holmes et al.*, 1968].

[21] At Prudhoe Bay, *Walker et al.* [1985] distinguished between steep-sided hydrostatic pingos (mean height 4 m, mean diameter 72 m, mean slope 7°) and broad-based mounds (mean height 5 m, mean diameter 242 m, mean slope 3°). Whether these broad mounds represent pingos is unclear, but drilling suggests at least the larger ones are ice cored [*Brockett*, 1982]. *Walker et al.* [1985] observed that the steep-sided pingos appear to be fairly randomly distributed in both the flat and gently rolling thaw-lake plains, whereas the broad-based mounds are clustered into regions of higher density within the gently rolling thaw-lake plains. We note two main groupings of these broad mounds, located to the east and west of the flat plains. We consider the steep-sided pingos as a third, separate group for NN analysis.

2.3. Candidate Martian Rootless Cones and/or Ice Mounds (10 Groups)

[22] For our third data set, we analyze ten groups of circular, subkilometer, positive topographic features of unknown origin from MOC-NA images at spatial resolutions of 3–6 m/pixel and THEMIS visible images at spatial resolutions of 17–74 m/pixel (Table 3). These groups (to which we will refer henceforth as ''candidate Martian groups'') were selected on the basis of their citation in the literature as candidates for rootless cones and/or ice mounds. Individual features range in basal diameter from ~15 to 1000 m, but are typically less than 300 m. Heights are more difficult to measure, but estimates based on individual Mars Orbiter Laser Altimeter (MOLA) measurements and photoclinometry suggest a range from just a few

Table 3. Examined Martian Feature Fields[a]

Image	Image Type	Image Number	Image Center (Lat., Long.)	Res.	Location (Sample, Line)
		Candidate Rootless Cone and/or Pingo Groups			
SE of Phlegra Montes (S)	M	M0801962	25.9°N, 170.3°E	5	300, 6100
SE of Phlegra Montes (N)	M	M0801962	25.9°N, 170.3°E	5	200, 7700
Cerberus Plains 1 (S)	M	M0800090	2.7°N, 143.9°E	6	250, 3900
Cerberus Plains 2 (Central)	M	M0800090	2.7°N, 143.9°E	6	150, 4550
Cerberus Plains 3 (N)	M	M0800090	2.7°N, 143.9°E	6	250, 5300
Acidalia Planitia	T	V05393016	40.3°N, 353.1°E	19	700, 1225
Isidis Planitia	T	V06251019	11.6°N, 84.8°E	18	500, 1650
Amazonis Planitia	M	M0700373	12.2°N, 196.3°E	3	225, 3400
Athabasca Valles	M	E1001384	9.6°N, 156.1°E	3	350, 5700
Gusev Crater	T	V01580003	14.5°S, 175.8°E	17	500, 825
(multiple images)	T	V02666002	14.1°S, 176.1°E	18	550, 900
	T	V05662001	14.0°S, 176.4°E	18	215, 2400
	T	V03777003	13.7°S, 175.9°E	18	455, 3210
		Secondary Impact Crater Groups			
Acidalia Planitia	T	V05393016	40.3°N, 353.1°E	19	25, 925
Ares/Tiu Valles	M	R1005447	19.9°N, 326.7°E	3	350, 4500
South Isidis Planitia	T	V01033003	3.9°N, 85.5°E	18	375, 925
Nili Fossae	T	V13927008	21.4°N, 76.3°E	37	300, 800
(multiple images)	T	V02394010	21.8°N, 76.3°E	37	300, 1325
	T	V02756003	21.3°N, 76.6°E	74	75, 1600
		Pedestal Crater Groups			
East of Acidalia Planitia 1	T	V13942006	46.3°N, 7.5°E	38	250, 2100
East of Acidalia Planitia 2	T	V13580002	47.5°N, 10.3°E	19	350, 1675
(multiple images)	T	V04993017	47.7°N, 10.0°E	19	550, 2300

[a]Image Type is M (MOC-NA) or T (THEMIS Visible); Res. is Image Resolution (meters/pixel); sample and line numbers are the x,y coordinates of the center of the feature field on the raw (unprojected) image.

meters at Athabasca Valles to close to 100 m at Gusev Crater [*Cabrol et al.*, 2000; *Burr et al.*, 2005; *Soare et al.*, 2005].

[23] Two of these candidate Martian groups are located southeast of Phlegra Montes and west of Amazonis Planitia (MOC-NA image M0801962). Here, features have been interpreted as rootless cones on the basis of a variety of criteria, including distinct conical morphology and well defined summit craters, stratigraphic position atop a lava flow having a pristine platy-ridged surface texture, the lack of association with eruptive fissures, and an absence of lava flows issuing from the cones [*Greeley and Fagents*, 2001; *Lanagan et al.*, 2001]. Three candidate Martian groups are located in the region *Plescia* [1990, 1993, 2003] called the Cerberus plains (MOC-NA image M0800090). These features have similarly been interpreted as rootless cones on the basis of distinctive morphologies and geologic relations [*Lanagan et al.*, 2001].

[24] The morphologies of cone-like features in the Cydonia region of Acidalia Planitia (THEMIS image V05393016) and within Isidis Planitia (THEMIS image V06251019) are less pristine. These two groups contain degraded, positive-relief, conical features with subdued summit craters (e.g., Figure 2a) that are quite distinct from the impact craters located within the same images. Cones and mounds in these areas were interpreted as rootless cones on the basis of Viking Orbiter imagery [*Frey et al.*, 1979; *Frey and Jarosewich*, 1982]. The surfaces on which the features reside appear considerably older than those in MOC-NA images M0800090 and M0801962, as evidenced by the higher density of impact craters. One possibility is that the cones formed on a sedimentary surface, in which case they could not be volcanic, let alone rootless. Alternatively, the original surface prior to mantling may have been lava that, in combination with a volatile-rich substrate, would admit the possibility of rootless cone formation. The Isidis cones have also been interpreted as pingos; their cratered expression has been attributed to ablation of ice cores within ice mounds [*Rossbacher and Judson*, 1981; *Grizzaffi and Schultz*, 1989]. However, the influx into the basin of voluminous flows from Syrtis Major (immediately to the west) suggests that significant lava resurfacing once took place and may have provided conditions favorable for rootless cone formation.

[25] In Amazonis Planitia, the confluence of recent volcanism and recent fluvial activity allows for the possibility of both pingo growth and rootless cone formation [*Burr et al.*, 2002a, 2002b]. MOC-NA image M0700373 shows a group of mounds and cones lying on an older, degraded surface. *Lanagan et al.* [2001] interpreted these mounds to be rootless cones.

[26] Recently acquired high-resolution MOC-NA images have revealed possible pingo forms in great detail. One particular group of features in Athabasca Valles (Figure 2b) has been imaged at resolutions as high as 1.5–3 m/pixel. Basal diameters lie in the range 15–128 m; heights are in the range 1.5–24 m [*Burr et al.*, 2005]. The continuum of morphologies exhibited in this image, ranging from circular mounds and pitted cones to irregularly shaped depressions with positive relief margins, is less characteristic of rootless volcanic cones. Furthermore, the association of these features with a sedimentary substrate in an outflow channel has been cited as corroborating evidence that these features are pingos, collapsing pingos, and residual pingo scars [*Burr et al.*, 2005]. An alternate interpretation for the low, rimmed depressions is that they are kettle holes or gravity craters [*Gaidos and Marion*, 2003].

[27] The final candidate Martian group is located along the margins of Thira Crater, located to the east of the Mars Exploration Rover, Spirit, landing site within Gusev Crater (Figure 3). On the basis of geomorphological interpretation of Viking Orbiter imagery, *Cabrol et al.* [2000] proposed these enigmatic mounds are pingos that formed shortly after the impact that created Thira Crater. Using higher resolution THEMIS visible imagery (V01580003; V02666002; V05662001; V03777003), we are able to identify 93 such mounds, almost three times the number originally identified by *Cabrol et al.* [2000].

2.4. Martian Impact Craters (6 Groups)

2.4.1. Martian Secondary Impact Craters (4 Groups)

[28] Of the six groups of Martian impact craters in our analysis, four represent probable secondary impact cratering events: Ares/Tiu Valles (imaged by MOC-NA at a resolution of 13 m/pixel), Acidalia Planitia, Nili Fossae, and south Isidis Planitia (all imaged by THEMIS at resolutions of 17–74 m/pixel) (Table 3). The largest craters are found at Nili Fossae, with diameters ranging up to 1.5 km. In the other three groups, craters are subkilometer in diameter. These features have been identified as probable secondary impact craters on the basis of their impact morphologies, occurrence in tight groupings and a qualitative inspection of their size-frequency distributions.

2.4.2. Martian Pedestal Craters (2 Groups)

[29] The final two groups of Martian impact craters included in this analysis have been previously identified as pedestal craters by other investigators [e.g., *Carr*, 1981]. Both groups are located just east of Acidalia Planitia, and were analyzed from THEMIS images at resolutions of 19–38 m/pixel (Table 3). Pedestal craters are believed to take on a highstanding expression when the surrounding surface undergoes substantial eolian erosion: the crater ejecta armors the underlying material, thereby protecting it from erosion. In some cases, pedestal crater ejecta take on broad, pancake-like morphologies. However, smaller examples with less extensive ejecta blankets are more conical, and hence more apt to be confused with volcanic cone structures.

[30] The six secondary and pedestal crater groups are included in this study to determine whether the spatial distributions of either or both impact crater types can be remotely distinguished from rootless cones and/or ice mounds. If the spatial distributions of these impact crater types are found to be statistically different from those of rootless cones and/or ice mounds, then NN analysis can be used to distinguish rootless cones and/or ice mounds from impact craters in images where morphology is not well defined due to degradation, modification or sediment cover. This assumes, however, that any such modification would not completely obliterate any feature or cause crater saturation, which would likely affect the spatial statistics. (See *Squyres et al.* [1997] for a discussion of the effect of crater saturation and obliteration on spatial statistics.)

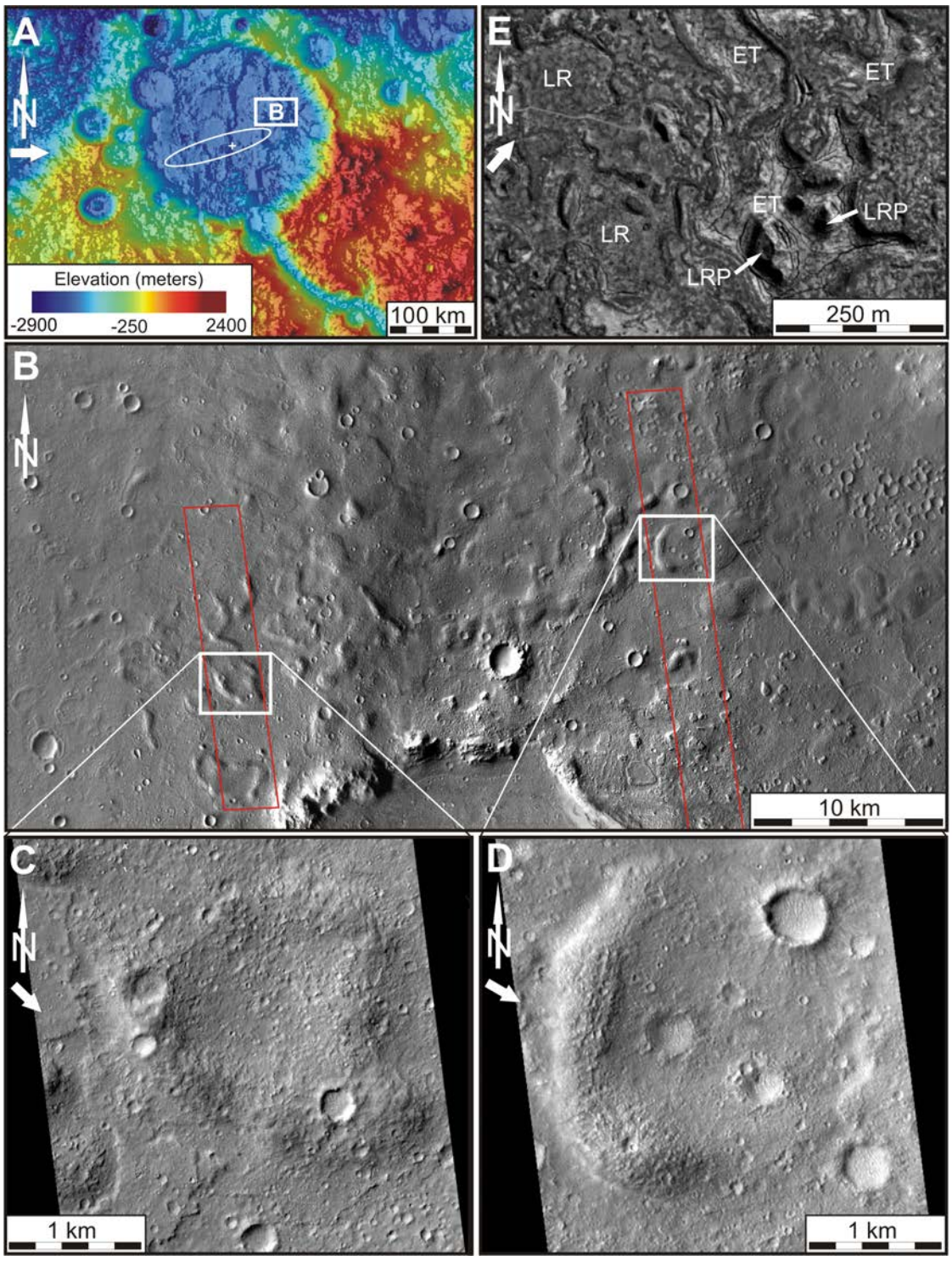

Figure 3. Mounds within Gusev Crater, Mars. (a) MOLA relief map showing the mound group location (white box). The landing ellipse and initial position of the MARS Exploration Rover Spirit are indicated. (b) Mosaic of THEMIS visible images depicting circular to elongate mounds just north of Thira Crater (V02666002, V03777003, V05662001, V12327003, V13238003, V14773003, V15085003). (c and d) Magnified views of two mounds that have circular curvature in plan view (MOC-NA images R22-01237, 2.98 m/pixel, and M02-02129, 5.96 m/pixel). (e) Lava inflation features in the Hrutagja flow, southwest Iceland, include elongate tumuli (ET) and lava-rise plateaus (LR) that surround lava-rise pits (LRP) [*Oskarsson*, 2005]. These inflation features may be analogous to the irregularly shaped, positive-relief features in Figure 3b and in the left-hand margin and lower left corner of Figure 3c. The illumination direction (180° from sun azimuth angle) is indicated by the broad white arrow.

[31] We note that other layered ejecta craters (e.g., single-layer, double-layer, or multiple-layer ejecta craters) [*Barlow et al.*, 2000], which are thought to form by emplacement of fluidized ejecta flows due to the presence of volatiles in the substrate [*Carr et al.*, 1977; *Gault and Greeley*, 1978; *Mouginis-Mark*, 1987] or through atmospheric effects [*Schultz and Gault*, 1979; *Schultz*, 1992; *Barnouin-Jha and Schultz*, 1996, 1998], typically exceed 4 km in diameter and exhibit quite distinctive morphologies. These craters are therefore unlikely to be mistaken for the subkilometer scale of rootless cones, pingos, and other ice mounds, and are not included in our analysis.

3. Methodology

3.1. Review of Standard Nearest Neighbor Methodology

[32] The NN technique quantifies the degree of spatial randomness of features within a plane and provides a means for evaluating the statistical significance of deviations from purely random. For detailed information on this method, including the underlying equations and derivations, refer to *Clark and Evans* [1954]. This technique can readily be applied to any feature type (e.g., primary or rootless volcanic cones, ice mounds, impact craters, lakes, kettle holes): it simply requires a map or image in which each feature is represented by a point. This methodology involves first measuring r, the distance between each point and its NN. In cases where cones contain multiple craters, each crater is considered to be a separate feature. We then average these distances together to arrive at R_a, the average *actual* distance between each pair of NNs:

$$R_a = \frac{\Sigma r}{n} \tag{1}$$

where n is the number of features in the group. (All equations are from *Clark and Evans* [1954].) Next, we calculate R_e, the average NN spacing that would be *expected* if the same number of features were distributed at random throughout the given field area:

$$R_e = \frac{1}{2\sqrt{\rho}} \tag{2}$$

where ρ is the density of the feature field (i.e., number of features divided by field area). The ratio of R_a and R_e yields the dimensionless statistic R, which quantifies any departure from the expected random spacing of nearest neighbors, i.e.,

$$R = \frac{R_a}{R_e} \tag{3}$$

By definition, randomly distributed cones would be expected to have $R_a \sim R_e$, yielding $R \sim 1$. Large values of R ($R > 1$) indicate that features are spaced further apart than would be expected from a Poisson NN distribution (i.e., $R_a > R_e$), as exemplified, in the limit, by a distribution of evenly spaced features. Small values of R ($R < 1$) reflect intragroup clustering: within a given group, features tend to occur more closely than would be expected at random (i.e., $R_a < R_e$).

[33] The key test statistic for evaluating whether an observed distribution is consistent with a random Poisson distribution is c:

$$c = \frac{R_a - R_e}{\sigma_{R_e}} \tag{4}$$

where σ_{R_e} is the standard error of the mean of the NN distances in a randomly distributed population. At the 0.05 significance level, the critical value of c is 1.96: $|c| > 1.96$ indicates statistically significant nonrandomness.

3.2. Field Area Selection

3.2.1. Convex Hull Methodology and Treatment of Border Features

[34] In their study of rootless cone groups, *Bruno et al.* [2004] defined the field area as the smallest external rectangle containing all cones in the field. However, by requiring the area to be rectangular, some degree of "empty space" was inherently added to each cone field. Moreover, field shape had an unintended influence on the final result, with rectangular fields having less dead space (and therefore tending to appear less clustered) than other field shapes.

[35] In this paper, we use the "convex hull" to define the natural boundary of a feature field [*Graham*, 1972]. This provides an improvement over prior analysis by diminishing areas in images that can distort statistical testing of spatial randomness. Here, the field area is defined as a convex polygon (i.e., a polygon with each interior angle measuring less than 180°), whose vertices are determined by the outermost features in the field. The convex hull is therefore the smallest convex polygon containing all features within a field and its perimeter will be the shortest path enclosing all points [*Graham*, 1972].

[36] Features which occur along the external edges of the group (i.e., lie on the convex hull) are selectively excluded from the analysis due to our inability to confidently locate their NN, which might lie beyond the edge of the image. These border features may serve as a NN to an interior feature, but they are excluded from the set of points that select a NN. For consistency, we apply this treatment to all border features for all feature fields, even in those cases where we are confident that all features are contained in the image. Figure 4 illustrates the convex hull methodology and treatment of border features on sample synthetic and natural data.

3.2.2. Spatial Subsets and Cluster Definition

[37] Depending on the distribution, the NN methodology can be highly sensitive to choice of spatial subset (Figure 4, Table 4). For self-similar (e.g., Poisson and evenly spaced) distributions, choosing a subset of the feature field should have little effect on NN results provided there are a sufficiently large number of features. Exactly how many features are required for a robust analysis is unclear. Table 4 suggests that 30 or 40 features may be sufficient, provided that the spatial distribution of the subset is representative of the feature field as a whole. However, if only a spatial subset of the feature field is available for analysis (e.g., due to limited imaging or mapping), it is impossible to discern whether the available data constitutes a representative subset so NN results cannot be generalized to the entire feature field.

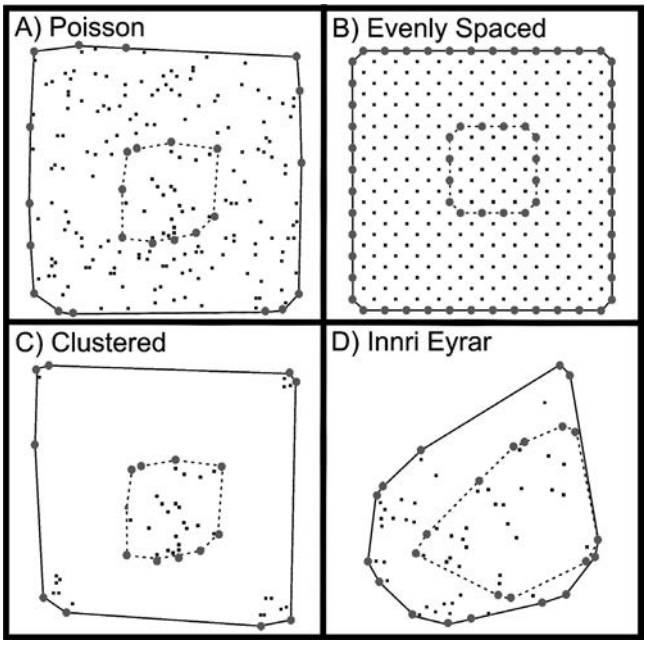

Figure 4. Illustration of the nearest neighbor (NN) technique and the effect of subsetting on three synthetic distributions (Poisson, evenly spaced and clustered) and one natural data set (Innri Eyrar, a rootless cone group, where each feature is represented by a dot). For each distribution, both the entire field area and a central spatial subset of 30–40 features are outlined with a convex hull. The detailed NN results are given in Table 4. (a) Poisson distribution. Both the entire field and spatial subset have R $\sim$ 1 and |c| < 1.96). (b) Evenly spaced distribution. Both the entire field and spatial subset have R > 1 and |c| > 1.96). (c) Clustered distribution. Unlike Figures 4a and 4b, NN results vary strongly with subsetting. The entire field area (composed of multiple clusters) shows significant aggregation (R < 1 and |c| > 1.96), whereas the spatial subset (central cluster only) is consistent with a Poisson NN distribution (R $\sim$ 1 and |c| > 1.96). (d) Innri Eyrar. Both the entire field and spatial subset have R < 1 and |c| > 1.96.

[38] As expected for both the entire field area and a spatial subset, Poisson NN distributions (Figure 4a) have $R \sim 1$ and $|c| < 1.96$, whereas evenly spaced distributions (Figure 4b) have $R > 1$ and $|c| > 1.96$ (Table 4). However, for clustered distributions, choosing a subset can have a considerable impact on NN results. Consider a feature field composed of multiple clusters (Figure 4c). Defining a feature field as encompassing multiple clusters (and hence considerable empty space between clusters) results in a low R value because the denominator R_e exceeds the numerator R_a. Restricting the feature field to one cluster has no systematic effect on R_a yet markedly decreases R_e, thereby increasing R. In the example shown in Figure 4c, R increases from 0.47 (full field of view encompassing five clusters) to 1.02 (central cluster only), the latter value reflective of a Poisson NN distribution. For comparison, NN results for sample natural data are also included (Figure 4d, Table 4). As is the case of Poisson and evenly spaced distributions, choosing a spatial subset of the original data set has little effect on NN results. This clearly results, though, from both the lack of multiple clusters within the data set (versus Figure 4c) as well as the fact that the selected subset had a similar spatial distribution to the feature field as a whole. We note, however, that all cases in Figure 4 are, in fact, finite, and the simple reality of the boundary may affect our conclusions, even when the distributions are Poisson or evenly spaced.

[39] In cases where a feature field appears to contain two or more clusters of features, we analyze each cluster separately. The definition of clusters is somewhat subjective; however, our choices are based on the physical context of each scene (e.g., natural geographical and geological boundaries such as coastlines, scarps, and lava flow margins). This follows from our motivation to explore the relationship between features *within* each cluster. Obviously, the features that we are studying occur in clusters. If we were to define a group as containing multiple clusters, NN results would necessarily show $R < 1$ (Figure 4c). Instead, we wish to explore what happens within each cluster: Do features form independently of one another? Do features preferentially form near preexisting ones? Or, conversely, does the existence of features in a given location serve to deter (“repel”) other features from forming nearby, perhaps implying competition for limited resources?

3.3. Skewness-Kurtosis Relation

[40] Standard NN methodology essentially reduces all the information in a feature field to two statistics (R and c). In this process, important information is lost regarding the detailed spatial distribution of features within the field. Two feature fields could easily have the same R and c values yet very different spatial arrangements of features. In the interest of developing a robust remote sensing tool to differentiate feature fields with similar R and c values, we examine the raw (i.e., unscaled) distances between each pair of NN to further characterize the spatial distribution of features. In particular, we examine the relationship between the third (skewness) and fourth (kurtosis) central moments of the distribution of pairwise NN distances. Skewness is a measure of asymmetry. Data skewed to the left have

Table 4. Effects of Field Area Selection on NN Results[a]

	N	N_b	R	c
Synthetic Poisson Distribution (Figure 4a)				
Spatial subset	31	10	1.02	0.21
Entire field	411	21	1.00	0.05
Synthetic Evenly Spaced Distribution (Figure 4b)				
Spatial subset	40	16	1.71	6.64
Entire field	312	48	1.91	28.39
Synthetic Clustered Distribution (Figure 4c)				
Spatial subset (within one cluster)	36	10	1.02	0.22
Entire field (several clusters)	60	10	0.47	−7.13
Sample Natural Data – Innri Eyrar (Figure 4d)				
Spatial subset	37	13	0.77	−2.14
Entire field	69	13	0.81	−2.68

[a] N, number of points in data set; N_b, number of points that lie on the convex hull; R, ratio of the mean nearest neighbor distance (R_a) to that expected of a Poisson distribution (R_e); c, statistical confidence in the departure from randomness ($|c| > 1.96$ indicates result is significant at the 0.05 level).

negative skewness, whereas data skewed to the right have positive values. Kurtosis is the degree of peakedness of a distribution; higher values indicate distributions with simultaneously sharper peaks and fatter tails. As these moments distinguish standard distributions from each other, this aspect of the methodology is designed to rapidly differentiate the NN distributions from each other without a detailed analysis of the full histogram of NN distances. There are a variety of formulae to estimate the skewness and kurtosis of distributions. We use the following fairly standard formulations:

$$\text{Skewness } \frac{n}{(n-1)(n-2)} \sum_{i=1}^{n} \left(\frac{r_i - R_a}{s} \right)^3 \quad (5)$$

Kurtosis

$$\left[\frac{n(n+1)}{(n-1)(n-2)(n-3)} \sum_{i=1}^{n} \left(\frac{r_i - R_a}{s} \right)^4 \right] - \frac{3(n-1)^2}{(n-2)(n-3)} \quad (6)$$

where r_i is the pairwise NN distance (computed for each feature in the field), R_a is the average NN distance in the feature field and s is the sample standard deviation. Using these definitions, a Gaussian distribution has skewness = 0 (i.e., is symmetric) and kurtosis = 0 (the peakedness of a bell-shaped curve). Before applying these formulae, pairwise NN data are trimmed by 5%, to minimize the influence of extreme high-end values, as discussed below.

4. Results

[41] Nearest neighbor results are summarized in Table 5 for terrestrial data sets and Table 6 for Martian data sets and are detailed below.

4.1. Terrestrial Data Sets

[42] Nearest neighbor analysis of the eight Icelandic rootless cone groups (Table 5) yields R values between 0.59 and 0.94 (mean $\bar{R} = 0.78$; standard deviation $s = 0.12$). In all cases, $R < 1.00$, indicating aggregation of cones within each group. All but two $|c|$ values exceed 1.96, which implies a significant departure from randomness at the 0.05 level for most groups. On average, the distance between a cone and its nearest neighbor is only 78% of that expected from a random spatial distribution. Blagil and Raudholar show lesser degrees of clustering ($R = 0.90$ and $R = 0.94$, respectively), which cannot be statistically distinguished from randomness. This does not necessarily imply that fundamentally different processes controlled the spatial distribution of features within these two feature fields; instead, it may simply represent the natural variation expected in natural data sets. Importantly, none of the Icelandic rootless cone groups show any evidence of "repulsion."

[43] Nearest neighbor analysis of the seven groups of ice mounds in Canada and Alaska gives R values ranging from 0.51 to 0.85 ($\bar{R} = 0.75$; $s = 0.12$), again indicating intragroup aggregation. High $|c|$ values (all > 1.96) attest that this clustering is statistically significant at the 0.05 level. At Prudhoe Bay, the two clusters of broad-based mounds (each $R = 0.78$) and steep-sided pingos ($R = 0.70$) show statistically similar degrees of clustering, supporting the argument that the broad mounds may represent pingos. These broad-based mounds cannot, however, simply be eroded steep-sided pingos, as they have much larger volumes [*Sedgewick*, 1990]. Unlike the broad mounds, the steep-sided pingos are not restricted to the gently rolling thaw-lake plains. However, *Walker et al.'s* [1985] observation that the steep-sided pingos are "fairly randomly distributed" is not supported by NN results, as the $|c|$ value of 10.94 well exceeds the critical value of 1.96. Like the broad-based mounds, the steep-sided pingos preferentially form near existing features.

[44] Similar R ranges of rootless cones (0.59–0.94) versus ice mounds (0.51–0.85) precludes differentiation between rootless cones and ice mounds based purely on R values. However, the skewness-kurtosis relationship described in section 3.3 above proves rather useful here. Skewness versus kurtosis for these two classes of features is shown in Figure 5a. Error bars are 2 standard errors of the mean (roughly corresponding to 95% confidence intervals). Although there is some overlap between skewness and kurtosis values for individual fields of these two feature types (Figure 5b), the distribution of NN distances for terrestrial ice mounds tends to be more skewed and leptokurtic (more peaked) relative to rootless cones. Such high skewness and leptokurtosis, reminiscent of an exponential probability distribution, implies that the formation of new features is influenced by the existence of earlier-formed features (as opposed to the Poisson distribution, where the probability of feature formation in a given region is solely dependent on area). Also shown in Figure 5 are data for Martian impact and nonimpact groups, which are discussed below.

[45] We note that the data presented in Figure 5 are trimmed. Our initial attempt to use skewness and kurtosis to discern rootless cones from ice mounds, based on the

Table 5. Results of Nearest Neighbor Analysis on Terrestrial Data Sets[a]

	N	N_b	R	c	*Skew*	*Kurt*
Icelandic Rootless Cone Groups						
Blagil	87	13	0.90	−1.68	0.64	0.21
Innri Eyrar	69	13	0.81	−2.68	0.60	−0.27
Hnuta (North)	357	13	0.83	−6.15	0.86	0.17
Hnuta (South)	301	12	0.74	−8.52	0.90	0.31
Trollhamar	131	12	0.59	−8.66	1.35	1.13
Stakafell	192	11	0.66	−8.78	1.13	0.37
Raudholar	198	17	0.94	−1.56	0.54	−0.53
Landbrot	1282	23	0.77	−15.43	0.68	−0.04
Alaskan and Canadian Ice Mound Groups						
Tanacross	152	11	0.51	−11.15	1.99	4.31
Prudhoe Bay (steep)	376	16	0.70	−10.94	1.22	0.80
Prudhoe Bay (broad) - E	112	16	0.78	−4.14	1.74	2.90
Prudhoe Bay (broad) - W	287	12	0.78	−7.02	1.32	1.63
Western Tuktoyaktuk	282	13	0.80	−6.28	1.90	4.91
Central Tuktoyaktuk	665	20	0.85	−7.31	1.17	1.60
Eastern Tuktoyaktuk	213	9	0.83	−4.53	1.71	3.10

[a] N, number of cones or craters; N_b, number of cones or craters that lie on the convex hull; R, ratio of the mean nearest neighbor distance (R_a) to that expected of a Poisson NN distribution (R_e); c, statistical confidence in the departure from randomness ($|c| > 1.96$ indicates result is significant at the 0.05 level); *Skew* and *Kurt*, skewness and kurtosis, respectively, of the distribution of pairwise NN distances.

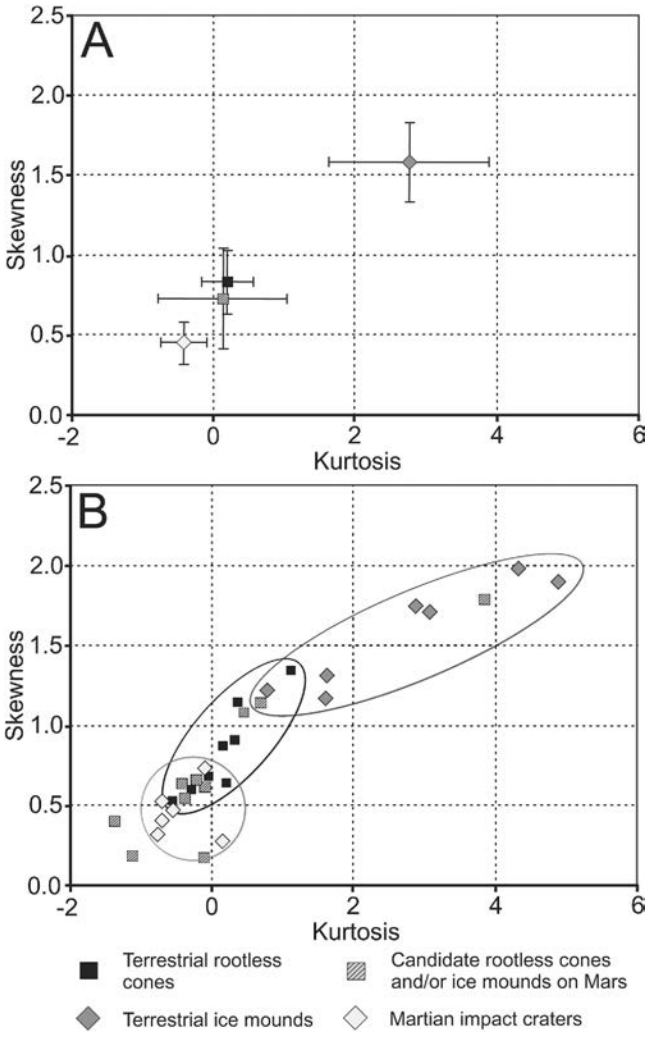

Figure 5. Results of skewness-kurtosis analysis. (a) Pooled data for four feature classes: terrestrial rootless cones (solid squares), terrestrial ice mounds (dark gray diamonds), candidate Martian rootless cones and/or ice mounds (hatched squares), and Martian impact craters (light gray diamonds). Mean skewness and kurtosis values are presented for each class. Vertical (skewness) and horizontal (kurtosis) error bars each represent ±2 standard errors of the mean. (b) Raw skewness and kurtosis data for each feature field studied. Ellipses are qualitative indicators of skewness-kurtosis ranges for each feature type. Both Figures 5a and 5b show that terrestrial ice mounds tend to have higher skewness and kurtosis values than both terrestrial rootless cones and candidate Martian groups.

entire (i.e., untrimmed) NN distribution, yielded ambiguous results. For rootless cones, kurtosis ranged from 2.89 to 60.36 (mean kurtosis = 14.32; s = 19.39) and skewness ranged from 1.35 to 5.20 (mean skewness = 2.52, s = 1.20). The respective ranges for ice mounds are 3.49 to 39.85 (mean kurtosis = 19.19, s = 14.85) and 1.82 to 5.31 (mean skewness = 3.56, s = 1.40). As the statistical distribution of geologic features reflects the physical processes that influenced feature formation [*Bruno et al.*, 2004; *Glaze et al.*, 2005], the NN distribution should bear some resemblance to classical probability distributions such as those associated with random processes, population growth and resource utilization. For comparison, the normal distribution has skewness and kurtosis values each of zero; the exponential distribution has corresponding values of two and six, respectively. Other classical probability distributions generally have similarly modest values of skewness and kurtosis. However, many of the feature fields included in this analysis have anomalously high values of skewness and kurtosis due to the influence of extreme high-end values.

[46] Extreme values suggest that features have been included in the data sets that belong to different statistical populations and/or were formed under different physical conditions. Visual inspection of the extreme values in the feature fields included in this analysis suggests they tend to be larger than average, and therefore may have caused a more pronounced depletion of local resources required for feature formation. Alternatively, they may have formed during different time periods, different ambient settings or by different physical processes that cannot be determined by a statistical analysis. Regardless, including extreme values inhibits our ability to distinguish feature types on the basis of skewness and kurtosis, as reflected in similar mean values and high standard deviations for rootless cones and ice mounds. Consequently, we have investigated these statistics using trimmed NN distributions. Statistical trimming is a standard technique [e.g., *Hoaglin et al.*, 1983] and is particularly useful in applications where influential factors have not been completely eliminated or controlled, as is clearly the case in the spatial distribution of geological features. We have found that excluding the highest 5% of values yields a remarkable separation between terrestrial ice mounds and rootless cones, and thus provides an important tool for interpreting the Martian data sets.

4.2. Martian Impact Crater Groups

[47] Nearest neighbor results for the four Martian secondary impact crater groups studied (Table 6) show R values in the 1.04–1.20 range ($\bar{R}$ = 1.12; s = 0.07). These results indicate that the spacing between craters within these crater groups is, on average, 12% greater than would be expected from a random distribution. Values of $|c|$ range from 0.65 to 4.49, with two of the four exceeding 1.96. Thus the spacing between craters, while always greater than random, can only be significantly discerned from randomness in two of the four cases.

[48] Similarly, the two Martian pedestal crater groups analyzed have R values of 1.00 and 1.07 ($\bar{R}$ = 1.04; s = 0.05). Both values of $|c|$ are less than 1.96, so neither of the two spatial distributions can be statistically distinguished from the Poisson NN distribution. Thus four of the six impact crater groups have random distributions, as might be expected from impact cratering processes. For the two groups with greater-than-random NN separations, it is unclear whether the craters formed preferentially away from existing features, or whether subsequent modification (such as crater obliteration) served to increase R.

[49] Critically, none of the six crater impact groups studied show any evidence of aggregation within a crater cluster (i.e., in all cases $R \geq 1.00$). Therefore they can be remotely distinguished from rootless cones and ice mounds purely on the basis of their degree of clustering (Figure 6).

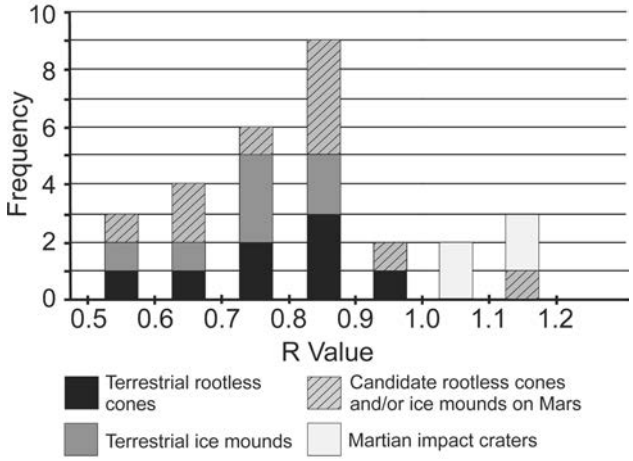

Figure 6. Summary of NN results for the four data sets studied in this analysis. All groups of terrestrial rootless cones and ice mounds show clustering ($R < 1.0$), whereas all Martian impact craters show spacing greater than or equal to that expected of a random distribution ($R \geq 1.0$). With a single exception, the NN results for the candidate Martian groups mirror those of the two terrestrial data sets. The exception (Gusev) has a distribution that is statistically indistinguishable from the impact craters.

Table 6. Results of Nearest Neighbor Analysis on Martian Data Sets[a]

	N	N_b	*R*	*c*	*Skew*	*Kurt*
Candidate Martian Rootless Cone and/or Ice Mound Groups						
SE of Phlegra Montes (S)	149	14	0.93	−1.66	0.19	−1.16
SE of Phlegra Montes (N)	282	17	0.86	−4.37	0.67	−0.24
Cerberus Plains 1	159	11	0.68	−7.54	1.79	3.83
Cerberus Plains 2	90	9	0.85	−2.63	1.09	0.45
Cerberus Plains 3	104	6	0.76	−4.64	0.63	−0.12
Acidalia Planitia	386	20	0.81	−6.91	0.64	−0.39
Isidis Planitia	247	13	0.66	−9.94	1.14	0.68
Amazonis Planitia	32	11	0.57	−3.78	0.41	−1.35
Athabasca Valles	891	15	0.83	−9.69	0.56	−0.41
Gusev Crater	104	11	1.18	3.31	0.19	−0.11
Martian Secondary Impact Crater Groups						
Acidalia Planitia	67	14	1.11	1.54	0.34	−0.76
Ares/Tiu Valles	196	17	1.15	3.95	0.48	−0.56
Nili Fossae	154	11	1.20	4.49	0.72	−0.08
South Isidis Planitia	94	9	1.04	0.65	0.29	0.18
Martian Pedestal Crater Groups						
East of Acidalia Planitia 1	257	15	1.00	0.07	0.51	−0.67
East of Acidalia Planitia 2	98	10	1.07	1.28	0.41	−0.70

[a] *N*, number of cones or craters; N_b, number of cones or craters that lie on the convex hull; *R*, ratio of the mean nearest neighbor distance (R_a) to that expected of a Poisson NN distribution (R_e); *c*, statistical confidence in the departure from randomness ($|c| > 1.96$ indicates result is significant at the 0.05 level); *Skew* and *Kurt*, skewness and kurtosis, respectively, of the distribution of pairwise NN distances.

This would be particularly useful for feature fields where morphology is not well-defined due to degradation, modification, or sediment cover.

4.3. Martian Candidate Rootless Cone and/or Ice Mound Groups

[50] The ten candidate Martian groups studied have *R* ranging from 0.57 to 1.18 ($\bar{R} = 0.81$; $s = 0.17$). The only feature field with $R > 1.00$ is found within Gusev Crater. Nearest neighbor results for these Gusev mounds ($R = 1.18$, $c = 3.31$) are markedly different from those of all other candidate Martian groups, as well as from the terrestrial groups of rootless cones and ice mounds. Unlike the rootless cones and ice mounds, which tend to cluster near each other, the Gusev mounds tend to form preferentially away from preexisting features. This "repulsion" is significantly different from random, as $|c|$ exceeds 1.96. Nearest neighbor results for the Gusev mounds fall within the range of the Martian impact crater groups studied in terms of both *R* (1.00–1.20) and *c* (0.07–4.49).

[51] Excluding the Gusev mounds leaves an *R* range of 0.57–0.93 ($\bar{R} = 0.77$; $s = 0.11$), with all but one $|c|$ value exceeding 1.96. These values are nearly identical to those obtained for both the Icelandic rootless cones ($\bar{R} = 0.78$; $s = 0.12$) and the terrestrial ice mounds ($\bar{R} = 0.75$; $s = 0.12$), yet show no overlap with the *R* range of the Martian impact crater groups studied (1.00–1.20). These NN results, summarized in Figure 6, lend support to the argument that the candidate Martian groups (except the Gusev mounds) may be rootless cones and/or ice mounds, but *R* and *c* values alone cannot be used to discriminate between these two possible origins. Thus, as in section 4.1 above, we examine the relationship between skewness and kurtosis.

[52] Skewness and kurtosis values for both individual feature fields and Mars candidate groups as a feature type are shown in Figure 5, alongside the terrestrial data. Immediately apparent from Figure 5a is the strong overlap in the skewness-kurtosis relationship between the candidate Martian groups and the terrestrial rootless cones, although the Martian data have more variance. The near coincidence of the mean skewness and kurtosis values of these two groups suggests they are drawing from the same population (i.e., that the candidate Martian groups are rootless cones). Detailed examination of the skewness-kurtosis relation of individual candidate Martian groups (Figure 5b; Table 6) reveals a somewhat more complex picture. One candidate Martian group (Cerberus Plains 1) has skewness and kurtosis values falling well within the range of terrestrial ice mounds. Two others (Cerberus Plains 2 and Isidis Planitia) have values intermediate between terrestrial rootless cones and ice mounds. Four groups (SE of Phlegra Montes N, Cerberus Plains 3, Athabasca Valles, and Acidalia Planitia) have skewness and kurtosis values well within the rootless cone range. This result, together with the *R* and *c* values of Table 6, suggests these four groups represent rootless cones. The same argument may hold for Amazonis Planitia and SE of Phlegra Montes (S), as their low skewness and kurtosis values suggest an ice mound origin is unlikely; however their skewness and kurtosis values are lower than any terrestrial rootless cone group. The final group (Gusev) has skewness and kurtosis values comparable to those of Martian impact craters, which further suggests that these mounds may represent modified impact craters (as discussed below).

5. Discussion

5.1. Improved Methodology

[53] Using an improved NN methodology, we have examined the spatial distribution of rootless cones in Ice-

Table 7. Comparison of *R* Values With Previous Nearest Neighbor Results[a]

	R Range (This Study)	*R* Range [*Bruno et al.*, 2004]
Icelandic rootless cone groups	0.59–0.94	0.57–0.88
Candidate Martian rootless cone groups	0.66–0.93	0.66–0.85
Martian impact crater groups	1.04–1.20	0.92–1.17

[a]Ranges of *R* values show comparison between two different NN methodologies. Only those data sets common to both studies are included.

land, ice mounds in Canada and Alaska, candidate rootless cones and ice mounds on Mars, and pedestal and secondary impact craters on Mars. Our approach invokes four spatial statistics (*R*, *c*, skewness, and kurtosis) and provides systematic methods for defining the cluster boundary (i.e., choosing a logical area and then constructing a convex hull) and treating border features (i.e., selectively excluding those features that lie on the hull boundary). We have shown that *R* and *c* values (the standard NN statistics) separate impact craters from rootless cones and ice mounds, but similar degrees of clustering preclude differentiation between the latter two feature types (Figure 6). This is where the skewness-kurtosis relation proves useful. The skewness and kurtosis of the NN distribution provides a remarkable segregation and grouping of terrestrial and Martian features for a trivial amount of computation. What is most significant is that this segregation and grouping emerges without the need for the postulation of an underlying probability distribution.

[54] The *R* values presented in this paper, on the basis of the refined methodology, are generally consistent with (but somewhat higher than) those of *Bruno et al.* [2004] for the identical data sets (Table 7). The slight differences are largely attributed to using the convex hull to define a cluster boundary, which eliminates empty space surrounding a feature field. Empty space increases R_e and therefore tends to decrease *R*; thus the elimination of space via the convex hull would conversely tend to increase *R*. A sensitivity analysis has shown that our selective treatment of border features had a much less pronounced effect on *R*, presumably because of the relatively large ratio of interior to border features which characterize these reasonably large data sets.

5.2. Interpretation of Martian Data Sets

[55] With a single exception, nearest neighbor results for the candidate Martian groups show $R < 1$, mirroring the results of terrestrial rootless cone and ice mound groups. These candidate Martian groups do not appear to represent impact craters, as all Martian secondary and pedestal impact crater groups studied have $R \geq 1$. Instead, these results suggest that, purely on the basis of their spatial distribution, these candidate Martian groups resemble ice mounds or rootless cones. Further discrimination between these two feature types is suggested on the basis of the relationship between skewness and kurtosis, as ice mounds tend to have higher values of both central moments. We do not attempt to argue convincingly that the candidate Martian groups are clusters of ice mounds or rootless cones, or whether ice mounds would even be expected on Mars. We simply note that both theories of origin are consistent with the results of our analysis, and warrant further examination in conjunction with other lines of evidence such as morphology, geological context (e.g., identifiable lava surface texture or water-bearing sediments), and physical constraints on their formation and preservation.

[56] The sole exception is the Gusev Crater mounds, whose NN results (*R*, *c*, skewness and kurtosis) are statistically indistinguishable from the Martian impact crater groups studied. These mounds were initially identified as pingos on the basis of geomorphological interpretation of Viking Orbiter imagery [*Cabrol et al.*, 2000]. However, more recent, higher-resolution THEMIS and MOC-NA imagery has failed to resolve any morphological characteristics that are diagnostic of pingos (Figures 3a–3d). *Mellon et al.* [2004] demonstrated that near-surface ground ice is currently unstable in the Gusev Crater region and the Mars Exploration Rover Spirit has revealed basalt to be the dominant surface lithology [*Squyres et al.*, 2004]. *Martínez-Alonso et al.* [2005] noted that both the morphology and dimensions of the Gusev mounds are consistent with those of inflated lava flows. Combining statistical and morphological lines of evidence, we speculate that the Gusev mounds may represent topographic inversion of impact craters due to lava flow inflation. Sites of localized inflation often originate as topographic lows into which lava concentrates [*Hon et al.*, 1994]. Continued accumulation of lava causes the surface of the flow to swell upward and may create features such as tumuli, lava-rise plateaus, and lava-rise pits [*Walker*, 1991]. These lava inflation features may be analogous to the Gusev mounds in that they initiated in topographic lows and topographically inverted the landscape into a series of circular to elongate ridges and plateaus (Figure 3e). In any case, the geospatial statistics and morphologies of the Gusev mounds distinguish them from rootless cones and ice mounds, thus suggesting a different formation mechanism.

5.3. Implications for Nonrandom Processes

[57] All 15 groups of terrestrial ice mounds and rootless cones studied show intragroup aggregation (all $R < 1$), i.e., features are more closely spaced than would be expected from a random spatial distribution. In all but two cases, this departure from randomness is statistically significant on the basis of an evaluation of *c*. This clustering implies that nonrandom processes systematically control the spatial distribution of rootless cones and ice mounds within their respective groups.

[58] For rootless cones, a likely control is the geometry of preferred lava pathways, evidenced by the presence of significant linear cone alignments and supported by field observations of Icelandic rootless cones [*Bruno et al.*, 2004]. Heterogeneous subsurface hydrology may also play a role in controlling cone distribution. Rootless cones form in lake basins, river floodplains, and glacial outwash plains [*Fagents et al.*, 2002], which presumably contain abundant water. If water was heterogeneously distributed within the substrate (e.g., by structural, lithological or hydrological controls) then this would limit the potential locations at which cones could form and influence broader-scale groupings within a flow field.

[59] Hydraulic pingos, such as those found in Tanacross, tend to form in narrow valleys or on slopes where perma-

frost is discontinuous or locally thinner. Thus a clustered distribution may simply reflect preferred locations of discontinuous or locally thinner permafrost. For hydrostatic pingos (e.g., Prudhoe Bay and Tuktoyaktuk Peninsula) which form following rapid drainage of lakes, a clustered distribution could either reflect (1) a nonrandom distribution of thaw-lake basins (e.g., thaw-lake locations could be controlled by the presence of drainage networks and drainage barriers) and/or (2) a nonrandom process that affects which thaw-lakes are capable of generating pingos (e.g., variable basin substrates may locally favor or prohibit the hydrological conditions required for pingo growth).

6. Conclusions

[60] We have shown that the spatial statistics of geologic features can be an effective supplement to geologic context and morphologic diagnostics to remotely differentiate between feature types such as rootless cones, ice mounds, and impact craters. Our method is based in part on the two statistics of the conventional nearest neighbor approach, R and c, which alone distinguish impact craters from the other two feature types. With a single exception, the R and c values of candidate Martian groups mirror those of terrestrial rootless cones and ice mounds. To further differentiate between these two feature types, we invoke the skewness-kurtosis relation, as ice mounds tend to have higher values of both central moments.

[61] The skewness-kurtosis statistic generally favors a rootless cone origin for the candidate Martian groups, although ice mounds remain a viable possibility for several groups. On the basis of NN results (as well as morphology), these Martian groups are clearly not clusters of impact craters: impact craters have distinctly different spatial distributions. The sole exception is the Gusev Crater mounds, which have R, c, skewness, and kurtosis values that are indistinguishable from those of Martian impact craters.

[62] In summary, we have developed an improved method for characterizing the spatial distribution of candidate rootless cones and ice mounds on Mars and quantitatively comparing them with terrestrial analogs. These results provide a basis for detailed physical modeling of the processes that form fields of these features and wider systematic applications may provide improvements in our understanding of the volatile inventory and evolution on Mars.

Notation

- c statistical measure of confidence in the departure from randomness.
- n number of features in the feature field.
- r distance between a feature and its nearest neighbor, [L].
- R statistical measure of departure from randomness of spatial distribution, = R_a/R_e.
- $\bar{R}$ average R value (for multiple feature fields).
- R_a average distance between nearest neighbors, [L].
- R_e average nearest neighbor spacing expected for a spatially random distribution [L].
- s sample standard deviation [L].
- ρ spatial density of features within a field, [L^{-2}].
- σ_{R_e} standard error of the mean of nearest neighbor distances in a randomly distributed population [L].

[63] **Acknowledgments.** We thank all those who shared their knowledge and provided insights, including T. Thordarson (rootless cones and lava inflation), E. Pilger (programming), and S. Still (clustering). Thorough reviews by L. Glaze and P. Lanagan led to significant improvements in this manuscript. This work was supported in part by NASA Mars Data Analysis Program grant NAG5-13458 to S.A.F. This paper is HIGP contribution 1436 and SOEST contribution 6774.

References

Allen, C. C. (1979a), Volcano-ice interactions on Mars, *J. Geophys. Res.*, *84*, 8048–8059.

Allen, C. C. (1979b), Volcano-ice interactions on the Earth and Mars, Ph.D. thesis, 131 pp, Univ. of Arizona, Tucson.

Barlow, N. G., J. M. Boyce, F. M. Costard, R. A. Craddock, J. B. Garvin, S. E. H. Sakimoto, R. O. Kuzmin, D. J. Roddy, and L. A. Soderblom (2000), Standardizing the nomenclature of Martian impact crater morphologies, *J. Geophys. Res.*, *105*, 26,733–26,738.

Barnouin-Jha, O. S., and P. H. Schultz (1996), Ejecta entrainment by impact-generated ring vortices: Theory and experiments, *J. Geophys. Res.*, *101*, 21,099–21,115.

Barnouin-Jha, O. S., and P. H. Schultz (1998), Lobateness of impact ejecta deposits from atmospheric interactions, *J. Geophys. Res.*, *103*, 25,739–25,756.

Brockett, B. E. (1982), Modification of and experience with a portable drill, Prudhoe Bay, Alaska, spring 1982, 14 pp., memorandum, Cold Regions Res. and Eng. Lab., U.S. Army Corps of Eng., Hanover, N. H.

Bruno, B. C., S. A. Fagents, T. Thordarson, S. M. Baloga, and E. Pilger (2004), Clustering within rootless cone groups on Iceland and Mars: Effect of nonrandom processes, *J. Geophys. Res.*, *109*, E07009, doi:10.1029/2004JE002273.

Burr, D. M., J. A. Grier, A. S. McEwen, and L. P. Keszthelyi (2002a), Repeated aqueous flooding from the Cerberus Fossae: Evidence for very recently extant, deep groundwater on Mars, *Icarus*, *159*, 53–73.

Burr, D. M., A. S. McEwen, and S. E. H. Sakimoto (2002b), Recent aqueous floods from the Cerberus Fossae, Mars, *Geophys. Res. Lett.*, *29*(1), 1013, doi:10.1029/2001GL013345.

Burr, D. M., R. J. Soare, and J.-M. Wan Bun Tseung (2005), Young (late Amazonian), near surface, ground ice features near the equator, Athabasca Valles, Mars, *Icarus*, *178*, 56–73.

Cabrol, N. A., E. A. Grin, and W. H. Pollard (2000), Possible frost mounds in an ancient Martian lake bed, *Icarus*, *145*, 91–107.

Carr, M. H. (1981), *The Surface of Mars*, 232 pp., Yale Univ. Press, New Haven, Conn.

Carr, M. H., L. S. Crumpler, J. A. Cutts, R. Greeley, J. E. Guest, and H. Masursky (1977), Martian impact craters and emplacement of ejecta by surface flow, *J. Geophys. Res.*, *82*, 4055–4065.

Carr, M. J. (1976), Underthrusting and Quaternary faulting in northern Central America, *Geol. Soc. Am. Bull.*, *87*, 825–829.

Chapman, M. G., and K. L. Tanaka (2001), Interior trough deposits on Mars: Subice volcanoes?, *J. Geophys. Res.*, *106*, 10,087–10,100.

Clark, P. J., and F. C. Evans (1954), Distance to nearest neighbor as a measure of spatial relationships in populations, *Ecology*, *35*, 445–453.

Connor, C. B. (1990), Cinder cone clustering in the TransMexican volcanic belt: Implications for structural and petrologic models, *J. Geophys. Res.*, *95*, 19,395–19,405.

Connor, C. B., and B. E. Hill (1995), Three nonhomogeneous Poisson models for the probability of basaltic volcanism: Application to the Yucca Mountain region, Nevada, *J. Geophys. Res.*, *100*, 10,107–10,125.

Connor, C. B., C. D. Condit, L. S. Crumpler, and J. C. Aubele (1992), Evidence of regional structural controls on vent distribution: Springerville Volcanic Field, Arizona, *J. Geophys. Res.*, *97*, 12,349–12,359.

Fagents, S. A., and T. Thordarson (2006), Rootless volcanic cones in Iceland and on Mars, in *The Geology of Mars: Evidence From Earth-Based Analogues*, edited by M. G. Chapman and I. P. Skilling, Cambridge Univ. Press, New York, in press.

Fagents, S. A., P. D. Lanagan, and R. Greeley (2002), Rootless cones on Mars: A consequence of lava-ground ice interaction, in *Volcano-Ice Interaction on Earth and Mars*, edited by J. L. Smellie and M. G. Chapman, *Geol. Soc. Spec. Publ.*, *202*, 295–317.

Farrand, W. H., L. R. Gaddis, and L. Keszthelyi (2005), Pitted cones and domes on Mars: Observations in Acidalia Planitia and Cydonia Mensae using MOC, THEMIS, and TES data, *J. Geophys. Res.*, *110*, E05005, doi:10.1029/2004JE002297.

Frey, H., and M. Jarosewich (1982), Subkilometer Martian volcanoes: Properties and possible terrestrial analogs, *J. Geophys. Res.*, *87*, 9867–9879.

Frey, H., B. L. Lowry, and S. A. Chase (1979), Pseudocraters on Mars, *J. Geophys. Res.*, *84*, 8075–8086.
Gaidos, E., and G. Marion (2003), Geological and geochemical legacy of a cold early Mars, *J. Geophys. Res.*, *108*(E6), 5055, doi:10.1029/2002JE002000.
Gault, D. E., and R. Greeley (1978), Exploratory experiments of impact craters formed in viscous-liquid targets: Analogs for Martian rampart craters?, *Icarus*, *34*, 486–495.
Glaze, L. S., S. W. Anderson, E. R. Stofan, S. Baloga, and S. E. Smrekar (2005), Statistical distribution of tumuli on pahoehoe flow surfaces: Analysis of examples in Hawaii and Iceland and potential applications to lava flows on Mars, *J. Geophys. Res.*, *110*, B08202, doi:10.1029/2004JB003564.
Graham, R. (1972), An efficient algorithm for determining the convex hull of a finite planar point set, *Info. Proc. Lett.*, *1*, 132–133.
Greeley, R., and S. A. Fagents (2001), Icelandic pseudocraters as analogs to some volcanic cones on Mars, *J. Geophys. Res.*, *106*, 20,527–20,546.
Grizzaffi, P., and P. H. Schultz (1989), Isidis Basin: Site of ancient volatile-rich debris layer, *Icarus*, *77*, 358–381.
Hasenaka, T., and I. S. E. Carmichael (1985a), The cinder cones of Michoacan-Guanajuato, central Mexico: Their age, volume, distribution and magma discharge rate, *J. Volcanol. Geotherm. Res.*, *25*, 105–124.
Hasenaka, T., and I. S. E. Carmichael (1985b), A compilation of location, size and geomorphological parameters of volcanoes in the Michoacan-Guanajuato volcanic field, Mexico, *Geofis. Int.*, *24*, 577–608.
Heming, R. F. (1980), Patterns of Quaternary basaltic volcanism in the northern North Island, New Zealand, *N. Z. J. Geol. Geophys.*, *23*, 335–344.
Hoaglin, D. C., F. Mosteller, and J. W. Tukey (1983), *Understanding Robust and Exploratory Data Analysis*, 447 pp., John Wiley, Hoboken, N. J.
Holmes, G., D. Hopkins, and H. Foster (1968), *Pingos in Central Alaska*, 40 pp., *Geol, Surv. Bull. 1241-H*, U.S. Dept. of the Interior, Washington, D. C.
Hon, K., J. Kauahikaua, R. Denlinger, and K. Mackay (1994), Emplacement and inflation of pahoehoe sheet flows: Observations and measurements of active lava flows on Kilauea Volcano, Hawaii, *Geol. Soc. Am. Bull.*, *106*, 351–370.
Lanagan, P. D., A. S. McEwen, L. P. Keszthelyi, and T. Thordarson (2001), Rootless cones on Mars indicating the presence of shallow equatorial ground ice in recent times, *Geophys. Res. Lett.*, *28*, 2365–2368.
Lucchitta, B. K. (1981), Mars and Earth: Comparison of cold climate features, *Icarus*, *45*, 264–303.
Mackay, J. R. (1962), Pingos of the Pleistocene Mackenzie Delta area, *Geogr. Bull. 18*, pp. 21–63, Geogr. Branch, Mines and Tech. Surv., Ottawa, Canada.
Mackay, J. R. (1973), The growth of pingos, western Arctic coast, Canada, *Can. J. Earth Sci.*, *10*, 979–1004.
Mackay, J. R. (1979), Pingos of the Tuktoyaktuk Peninsula area, Northwest Territories, *Geogr. Phys. Quat.*, *33*, 3–61.
Mackay, J. R. (1987), Some mechanical aspects of pingo growth and failure, western Arctic coast, Canada, *Can. J. Earth Sci.*, *24*, 1108–1119.
Mackay, J. R. (1998), Pingo growth and collapse, Tuktoyaktuk Peninsula Area, western Arctic coast, Canada: A long-term field study, *Geogr. Phys. Quat.*, *52*, 271–323.
Martínez-Alonso, S., B. M. Jakosky, M. T. Mellon, and N. E. Putzig (2005), A volcanic interpretation of Gusev Crater surface materials from thermophysical, spectral, and morphological evidence, *J. Geophys. Res.*, *110*, E01003, doi:10.1029/2004JE002327.
Mellon, M. T., W. C. Feldman, and T. H. Prettyman (2004), The presence and stability of ground ice in the southern hemisphere of Mars, *Icarus*, *169*, 324–340.
Mouginis-Mark, P. J. (1987), Water or ice in the Martian regolith?: Clues from rampart craters seen at very high resolution, *Icarus*, *71*, 268–286.
Müller, F. (1959), Meddeleser on Grønland (in German), *153*(3), 127 pp. (translated by D. A. Sinclair, Natl. Res. Counc. of Can, Ottawa, Ont., 117 pp., 1963).
Oskarsson, B. V. (2005), Lava-rise structures in pahoehoe and àa: Examples from the Hrutagja lava shield and Kapelluhraun àa flow field on the Reykjanes Peninsula, B.Sc. thesis, Univ. of Iceland, Reykjavik.
Page, D. P., and J. B. Murray (2006), Stratigraphic and morphological evidence for pingo genesis in the Cerberus plains, *Icarus*, doi:10.1016/j.icarus.2006.01.017, in press.
Parker, T. J., D. S. Gorsline, R. S. Saunders, D. C. Pieri, and D. M. Schneeberger (1993), Coastal geomorphology of the Martian northern plains, *J. Geophys. Res.*, *98*, 11,061–11,078.
Plescia, J. B. (1990), Recent flood lavas in the Elysium region of Mars, *Icarus*, *88*, 465–490.
Plescia, J. B. (1993), An assessment of volatile release from recent volcanism in Elysium, Mars, *Icarus*, *104*, 20–32.
Plescia, J. B. (2003), Cerbereus Fossae, Elysium, Mars: A source of lava and water, *Icarus*, *164*, 79–95.
Porsild, A. E. (1938), Earth mounds in unglaciated Arctic northwestern America, *Geogr. Rev.*, *28*, 46–58.
Rossbacher, L. A., and S. Judson (1981), Ground ice on Mars; inventory, distribution, and resulting landforms, *Icarus*, *45*, 39–59.
Schultz, P. H. (1992), Atmospheric effects on ejecta emplacement, *J. Geophys. Res.*, *97*, 11,623–11,662.
Schultz, P. H., and D. E. Gault (1979), Atmospheric effects on Martian ejecta emplacement, *J. Geophys. Res.*, *84*, 7669–7687.
Sedgewick, R. (1990), *Algorithms in C*, 657 pp., Addison-Wesley Longman, Boston, Mass.
Settle, M. (1979), The structure and emplacement of cinder cone fields, *Am. J. Sci.*, *279*, 1089–1107.
Soare, R. J., D. M. Burr, and J.-M. Wan Bun Tseung (2005), Possible pingos and a periglacial landscape in northwest Utopia Planitia, *Icarus*, *174*, 373–382, doi:310.1016/j.icarus.2004.1011.1013.
Squyres, S. W., S. M. Clifford, R. O. Kuzmin, J. R. Zimbelman, and F. M. Costard (1992), Ice in the Martian regolith, in *Mars*, edited by H. H. Kieffer et al., pp. 523–554, Univ. of Ariz. Press, Tucson.
Squyres, S. W., C. Howell, M. C. Liu, and J. J. Lissauer (1997), Investigation of crater 'saturation' using spatial statistics, *Icarus*, *125*, 67–82.
Squyres, S. W., et al. (2004), The Spirit Rover's Athena science investigation at Gusev crater, Mars, *Science*, *305*, 794–799.
Stager, J. K. (1956), Progress report on the analysis of the characteristics and distribution of pingos east of the Mackenzie delta, *Can. Geogr.*, *7*, 13–20.
Tanaka, K. L. (1997), Sedimentary history and mass flow structures of Chryse and Acidalia Planitiae, Mars, *J. Geophys. Res.*, *102*, 4131–4419.
Theilig, E., and R. Greeley (1979), Plains and channels in the Lunae Planum–Chryse Planitia region of Mars, *J. Geophys. Res.*, *84*, 7994–8010.
Thorarinsson, S. (1951), Laxargljufur and Laxarhraun. A tephrochronological study, *Geogr. Ann.*, *H1–2*, 1–89.
Thorarinsson, S. (1953), The crater groups in Iceland, *Bull. Volcanol.*, *14*, 3–44.
Thordarson, T. (2000), Rootless eruptions and cone groups in Iceland: Products of authentic explosive water to magma interactions, in *Volcano/Ice Interactions on Earth and Mars, Abstract Volume*, edited by V. C. Gulick and M. T. Gudmundsson, p. 48, Univ. of Iceland, Reykjavik.
Thordarson, T., and A. Höskuldsson (2002), *Iceland*, Terra, Harpenden, Hertfordshire, U. K.
Thordarson, T., D. J. Miller, and G. Larsen (1998), New data on the Leidolfsfell cone group on south Iceland, *Jökull*, *46*, 3–15.
Thordarson, T., M. M. Morrissey, G. Larsen, and H. Cyrusson (1992), Origins of rootless cone complexes in S. Iceland, in *The 20th Nordic Geological Winter Meeting*, edited by A. Geirsdóttir, H. Norddahl, and G. Helgadóttir, p. 169, Icelandic Geol. Soc., Reykjavik.
Thoroddsen, T. (1894), Ferd un Vestur Skaftafellssyslu sumarid 1893 (Travelogue from Western Skaftafellshire in the summer of 1893), *Andvari*, *19*, 44–161.
Walker, D., M. Walker, K. Everett, and P. Webber (1985), Pingos of the Prudhoe Bay Region, Alaska, *Arctic Alpine Res.*, *17*, 321–336.
Walker, G. P. L. (1991), Structure, and origin by injection of lava under surface crust, of tumuli, "lava rises", "lava rise pits", and lava inflation clefts in Hawaii, *Bull. Volcanol.*, *53*, 546–558.
Walker, J. (1981), Petrogenesis of lavas from cinder cone fields behind the volcanic front of Central America, *J. Geol.*, *89*, 721–739.
Washburn, A. L. (1973), *Periglacial Processes and Environments*, 320 pp., Edward Arnold, London.

S. M. Baloga, Proxemy Research, 20528 Farcroft Lane, Bowie, MD 20882, USA.
B. C. Bruno, S. A. Fagents, and C. W. Hamilton, Hawai'i Institute of Geophysics and Planetology, University of Hawai'i, 1680 East West Road,POST 504, Honolulu, HI 96822, USA. (barb@hawaii.edu)
D. M. Burr, SETI Institute, 515 North Whisman Road, Mountain View, CA 94043, USA.